DOI: https://doi.org/10.14525/JJCE.v20i1.06



Jordan Journal of Civil Engineering

Journal homepage: https://jjce.just.edu.jo



Load-Bearing Capacity Analysis of Prestressed Concrete in Bridge Engineering Based on Cracks and Section Loss

Yu Pei 1), Ziyi Lyu 1)*, Lijuan Xie 2), Shimeng Liu 3)

- ¹⁾ Department of Road and Bridge Engineering, Hebei Jiaotong Vocational and Technical College, Shijiazhuang 050000, China. * Corresponding Author. Email: <u>Lzypy1120@163.com</u>
- 2) College of Mechanical and Electrical Engineering, Hebei Vocational College of Rail Transportation, Shijiazhuang 050000, China.
- ³⁾ Basic Teaching Department, Hebei Jiaotong Vocational and Technical College, Shijiazhuang 050000, China.

ARTICLE INFO

ABSTRACT

Article History: Received: 24/6/2025 Accepted: 21/8/2025

The load-bearing capacity analysis of pre-stressed concrete in bridge engineering is a core technology for structural safety evaluation. It has long faced challenges in insufficient detection accuracy under complex stress environments and low efficiency in multi-source data fusion. Traditional analysis methods rely on a single mechanical model or empirical experience, making it difficult to accurately capture the nonlinear relationship between crack development and load-bearing capacity degradation. Therefore, this study proposes a prestressed concrete load-bearing capacity analysis model based on a dual-threshold edge detection algorithm. Experimental results show that the accuracy of the improved edge detection algorithm reaches a maximum of 89.5% after iteration, with the misdetection rate of bridge cracks under various noise influences being as high as 9%. Evaluation of the fusion analysis model shows that the Mean Square Error (MSE) of its load-bearing capacity is only 0.015 kN·m², and the coefficient of determination R² is 0.98. These results indicate that the proposed prestressed concrete load-bearing capacity analysis model can effectively improve the prediction accuracy of load-bearing capacity under complex stress environments and accurately capture the nonlinear relationship between crack development and loadbearing capacity degradation. Compared with existing research, the core contributions of this study are reflected in three aspects: 1. A collaborative analysis framework for crack characteristics and section loss was constructed, quantifying the coupling influence mechanism of the two on bearing capacity and breaking through the limitations of traditional single-factor analysis; 2. A prestressed concrete bearing capacity analysis model was proposed. Through algorithms, the core characteristics of crack-section loss were precisely screened, and the problem of dynamic bearing capacity prediction under small samples was solved, filling the technical gap of nonlinear mapping in complex stress environments; 3. The experiment verified the quantitative correlation between crack size and steel bar damage (for every 0.1mm increase in crack width, the steel bar corrosion rate increases by approximately 15%), providing an operational quantitative method for inferring internal structural damage from surface cracks. This study provides a new technical approach for bridge structural safety assessment and contributes to the development of intelligent monitoring and full-life-cycle maintenance technologies for prestressed concrete structures.

Keywords: Bridge engineering, LSTM, Otsu, PSO, Crack characteristics, GAN.

INTRODUCTION

In recent years, the vigorous development of bridge engineering leads to the widespread application of prestressed concrete structures in various types of bridges due to their excellent bearing performance (Farneti et al., 2023). However, the impact of bridge cracks and the resulting cross-sectional loss on the bearing capacity of prestressed concrete becomes increasingly significant, making bridge cracks a key research topic in the field of bridge engineering (Ni et al., 2025). Accurately identifying cracks, extracting features, and monitoring bearing capacity are crucial to ensuring bridge safety and durability (Tonelli et al., 2023). Traditional detection methods have insufficient accuracy and poor adaptability in complex crack image recognition and feature extraction, making it difficult to meet the requirements of modern bridge engineering. An efficient and accurate processing solution is urgently needed. Therefore, this study proposes a new prestressed concrete bearing capacity analysis model, which takes into account crack recognition accuracy, feature extraction efficiency, and dynamic monitoring capabilities. In this model, the Canny Edge Detection Algorithm (Canny), improved by Otsu, combines the advantages of threshold segmentation and edge detection (Salunke et al., 2023), and the Particle Swarm Optimization (PSO) algorithm effectively extracts crack features and improves analysis accuracy (Demir et al., 2023). At the same time, the model also combines the Generative Adversarial Network (GAN) with Long Short-Term Memory (LSTM) to achieve dynamic time series monitoring of the bearing capacity of prestressed concrete. It is expected that this model can break through the limitations of traditional single detection and promote the development of bridge structure health monitoring towards precision and intelligence. This study innovatively integrates the neural network and the algorithm architecture, breaking detection inefficiency of traditional detection, and has important theoretical significance and engineering application value for improving the safety and durability of bridge engineering.

RELATED WORKS

The Otsu-Canny algorithm is an image edge

detection method that combines Otsu threshold segmentation and Canny edge detection. It is often used to extract target edges in images and is widely used in many fields. Scientists have conducted extensive discussions on this algorithm. For example, Ramadhan proposed an edge detection method using Otsu threshold and Canny edge to address the problem that lowresolution images often suffer from quality degradation and important details are lost due to noise and blur. Experimental results showed that this method had a lower loss value and was therefore recommended as a more effective method for low-resolution image processing (Ramadhan et al., 2025). Zhang et al. developed an adaptive segmentation approach that integrates the Otsu method with a dynamic Canny edge detection technique to mitigate the influence of external identification. disturbances on sea-sky line Experimental outcomes demonstrated that the proposed method maintained strong accuracy and robustness in handling images captured in complex maritime environments (Zhang et al., 2024). Xiong et al. proposed an improved Canny edge detection algorithm to solve the problems of low efficiency, susceptibility to human interference, and low measurement accuracy of traditional manual sorting and size measurement methods in the production process of photosynthetic devices. Experimental results showed that the algorithm achieved pixel center point positioning error compliance with the average execution time of 143.34ms (Xiong et al., 2025). Choi and Ha introduced a method for automatically selecting three suitable thresholds in the Canny edge detection algorithm by employing the actorcritic algorithm to address the thresholding issue. Experimental results across various datasets confirmed the practicality and effectiveness of the proposed algorithm (Choi & Ha, 2023). In response to the lack of early prevention and detection of breast tumor cases, Triwibowo et al. suggested applying the Canny edge detection algorithm to process breast X-ray images utilizing the Support Vector Machine method for classifying the types. The detection results showed that the classification accuracy was 95%. From the results obtained, it can be seen that the application system was very suitable for the early identification of breast tumors (Triwibowo et al., 2023).

With the large-scale development of infrastructure construction and the widespread application of

prestressed concrete materials, new theoretical models and analysis methods have been continuously proposed and applied in the field of prestressed concrete bearing capacity research. Engineers have carried out extensive studies in this area. For instance, Zhou et al. performed multi-stage variable amplitude fatigue tests on three groups of prestressed concrete beams with different sizes to investigate the fatigue damage mechanism of prestressed concrete beams under fatigue loads. The results indicated that the increase in residual bearing capacity of prestressed concrete beams decreased as the cross-sectional size increased (Zhou et al., 2025). In order to explore whether spun prestressed concrete piles could replace foundation solutions, Farzana et al. used various analysis methods and static pile load tests to estimate the vertical bearing capacity of spun prestressed concrete piles in the Jolshiri area of Dhaka, Bangladesh. The experiment showed that the prestressed piles had good substitutability (Farzana et al. 2024). Hu et al. built and tested eight beams under cyclic loading to evaluate the hysteresis performance of aramid fiber reinforced polymer prestressed concrete beams. The test variables included the type of prestressed tendons and the ratio of internal to external tendons. The experiment showed that the damage of all beams was mainly concrete crushing and non-prestressed steel bars ruptured in pure bending sections (Hu et al., 2024). Li et al. (2024) introduced a novel approach utilizing distributed acoustic sensing technology to monitor and detect wire breaks in prestressed concrete tubes, aiming to assess the condition of these tubes. The results showed that this method could quickly and effectively capture wire breaks and noise in various environments (Li et al., 2024). Gleich and Maurer proposed a shear analysis method to perform structural evaluation on existing old prestressed concrete bridges. Experimental results showed that the proposed concrete shear analysis method could more realistically determine the shear bearing capacity of prestressed beams compared to the truss model under the current standardized state (Gleich & Maurer, 2023).

To sum up, existing research has made certain progress in the analysis of the bearing capacity of prestressed concrete. However, there are three significant limitations in the current research: 1. Focus is more on the influence of a single factor (such as only

cracks or only section loss) on the bearing capacity, while ignoring the coupling effect of the two (for example, crack propagation accelerates the corrosion of steel bars, and corrosion in turn aggravates the development of cracks). 2. The correlation between cracks and steel bar damage is mostly described qualitatively, lacking quantitative models, making it difficult to infer the degree of internal steel bar section loss from the surface crack characteristics, 3. Traditional models have insufficient generalization ability in small sample sizes and complex noise environments, making it difficult to meet the dynamic monitoring requirements of actual bridges. The research integrates multiple algorithms based on actual needs to solve the above problems. The proposed prestressed concrete bearing capacity analysis model that combines neural networks and detection algorithms has good performance. It is expected that this model can promote the development of bridge structure health monitoring towards precision and intelligence.

Design of Prestressed Concrete Bearing Capacity Based on Crack Features and Section Loss Bridge Crack Identification and Feature Parameter Extraction Method Design

With the deep integration of intelligent monitoring technology for bridge engineering and health management of prestressed concrete structures, the need to accurately identify the impact of cracks on bearing capacity is becoming increasingly urgent (Usman & Abdullah, 2023). However, traditional detection methods are insufficient in capturing crack features and are easily disturbed by environmental noise, making it difficult to balance detection sensitivity computational efficiency (Alherbawi et al., 2023; Fan et al., 2024). In order to address the problems of nonlinear coupling of crack stress and low efficiency of multiscale crack feature recognition in prestressed concrete structures of bridges, the Canny detection algorithm is proposed. The algorithm dynamically optimizes edge responses by simulating the detection mechanism of biological visual edge perception, so that the crack identification process focuses more on the characteristic crack extension path caused by stress concentration. The structure of the Canny detection algorithm is shown in Figure 1.

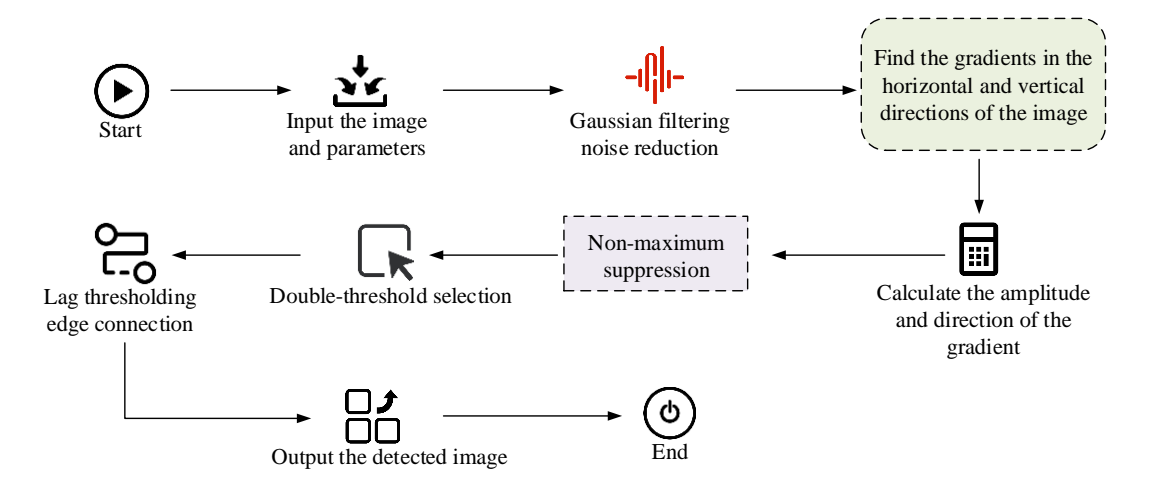


Figure 1. Structure diagram of Canny detection algorithm

As shown in Figure 1, the Canny detection algorithm first inputs the image and parameters, and then performs Gaussian filtering to reduce noise. Then, the horizontal and vertical gradients of the image are obtained, and the gradient amplitude and direction are calculated. Then, the non-maximum suppression step is entered, and then double threshold selection is performed, and edge connection performed through hysteresis thresholding. The above processing flow is repeated until all pixels are detected, and finally, the detected image is output. Gaussian filtering is used to smooth the image and remove noise. The definition of the twodimensional Gaussian function is shown in Equation (1).

$$H(x,y) = \frac{1}{2\pi\sigma^2} e^{-\frac{x^2 + y^2}{2\sigma^2}}$$
 (1)

In Equation (1), σ represents the standard deviation of the Gaussian kernel, controlling the smoothing degree, and x, y represent the center coordinates of the Gaussian function along the x and y axes. Next, in the gradient magnitude and direction calculation step, the Sobel operator is employed to compute the gradient in both the horizontal and vertical directions of the image. The horizontal and vertical Sobel operators are represented in Equation (2).

$$\begin{cases} G_x = \begin{pmatrix} -1 & 0 & 1 \\ -2 & 0 & 2 \\ -1 & 0 & 1 \end{pmatrix} \\ G_y = \begin{pmatrix} 1 & 2 & 1 \\ 0 & 0 & 0 \\ -1 & -2 & -1 \end{pmatrix}$$
 (2)

In Equation (2), G_x and G_y represent the Sobel operators in the horizontal and vertical directions, respectively, G is the gradient amplitude. Using these two equations, the gradient magnitude and direction are calculated, as shown in Equation (3).

$$G = \sqrt{G_x^2 + G_y^2 \theta} = \arctan\left(\frac{G_y}{G_x}\right)$$
 (3)

In Equation (3), θ represents the direction of the gradient. Although the Canny edge detection algorithm plays a role in processing bridge crack images, it still has limitations, such as relying on empirical double threshold selection, insufficient adaptability to complex images, and sensitivity to noise, making it difficult to suppress the irregular surface texture of concrete and monitoring noise interference (Syahifitri, 2023; Liu et al., 2024). Therefore, the introduction of the gradient-based dual-threshold Otsu algorithm is proposed, which resolves these issues through adaptive threshold computation based on gradient information, global pixel statistical feature analysis, and multi-scale edge fusion. The Otsu-Canny edge detection algorithm flow, combining Canny and Otsu, is shown in Figure 2.

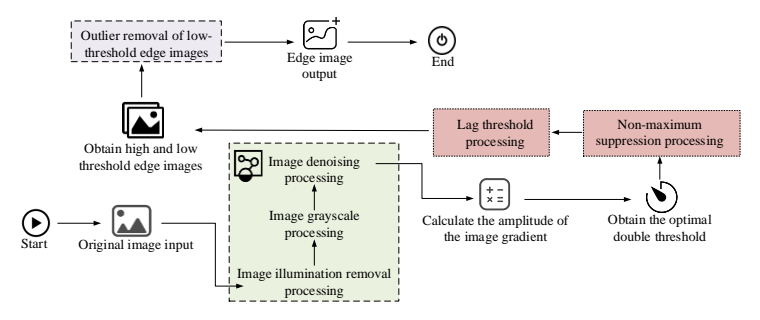


Figure 2. Otsu-Canny edge detection algorithm workflow diagram

In Figure 2, the Otsu-Canny algorithm first performs image preprocessing. Then, the image gradient amplitude is calculated, and the gradient double threshold Otsu algorithm is used to adaptively obtain the optimal double threshold. Then. non-maximum suppression implemented to refine the edge, and the strong and weak edges are distinguished by hysteresis threshold processing and irrelevant pixels are excluded to obtain high and low threshold edge images. Finally, isolated noise points in the low threshold edge image are removed to output an accurate edge image. The Otsu algorithm is an image binarization algorithm based on maximizing the inter-class variance. The total number of pixels in the image is usually related to the grayscale, as shown in Equation (4).

$$N = \sum_{i=0}^{L-1} N_i \tag{4}$$

In Equation (4), the number of pixels with grayscale value i is N_i , and L represents the number of grayscale levels. The probability of grayscale value i is the ratio of the total number of pixels to the number of pixels with grayscale value i. The image is subsequently segmented using the threshold, and the process for computing the foreground probability is outlined in Equation (5).

In Equation (5), t represents the threshold, and p_i represents the probability of grayscale value i. When processing an image with a lower threshold, both strong and weak edges of the target object will be detected, making the true edges appear relatively continuous. The isolated pixel points that appear are more likely to belong to discrete noise interference, and the between-class variance g is calculated as shown in Equation (6)

$$g = \omega_0 (\mu_0 - \mu)^2 + \omega_1 (\mu_1 - \mu)^2 = \omega_0 \omega_1 (\mu_0 - \mu_1)^2$$
 (6)

In Equation (6), ω_0 and ω_1 represent the foreground and background probabilities, respectively, while μ_0 and μ_1 refer to the average gray level, and μ represents the total average gray level of the image. Otsu-Canny searches through all possible thresholds to find the one that maximizes g, where the foreground and background differences are greatest, resulting in the best segmentation effect. After identifying bridge cracks, the study proposes using PSO for feature extraction to quantify the impact of cracks on the prestressed concrete bearing capacity of the bridge. In summary, the flow of the bridge crack recognition and feature parameter extraction method is shown in Figure 3.

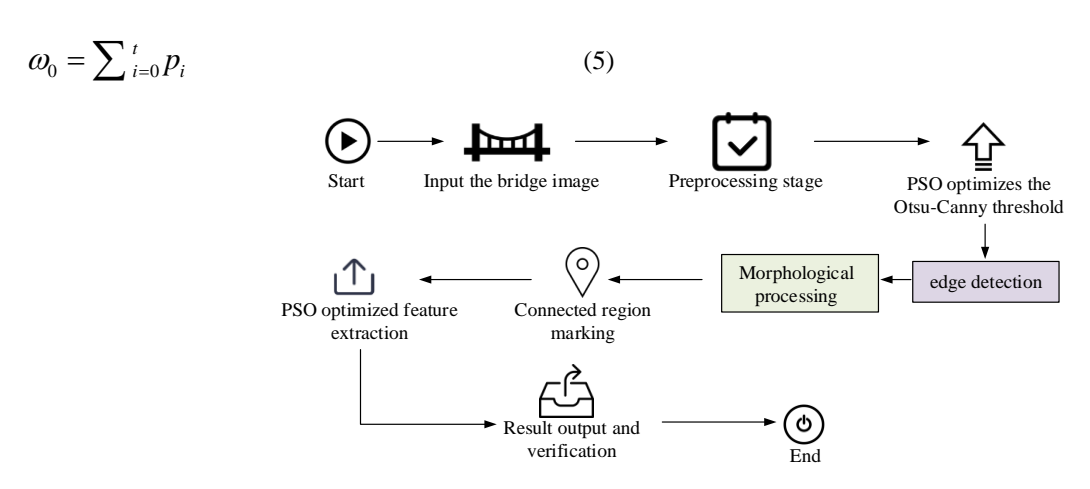


Figure 3. Bridge crack identification and characteristic parameter extraction method flow

As shown in Figure 3, the method first inputs the bridge image, then preprocesses it. Next, the PSO algorithm further optimizes the Otsu-Canny threshold, and the optimized algorithm performs edge detection on the image. After morphological processing and connected region labeling, the PSO algorithm is used to extract crack features, ultimately generating a visualized crack area and detection report.

Prestressed Concrete Bearing Capacity Analysis Model Construction

As mentioned earlier, crack characteristics and section loss can affect the load-bearing capacity of prestressed concrete through a synergistic effect, but the specific action path (how to aggravate section damage through crack development and how to infer the degradation of load-bearing capacity through section loss) remains unclear. To accurately construct a carrying capacity analysis model, it is necessary to first clarify the intrinsic correlation mechanism among the three. The core logic can be summarized as cascading influence and quantitative feedback :1. Crack \rightarrow Section loss: When the crack width exceeds 0.2mm, external moisture and chloride ions invade the surface of the the crack, reinforcing bar along accelerating electrochemical corrosion. As the crack width increases, the corrosion rate of the reinforcing bars rises, and the cross-sectional loss rate of the reinforcing bars (corrosion area/original area) increases after 6 months. If surface cracks in concrete are accompanied by forking (the number of forking ≥ 2), this will lead to an expansion of the local spalling area, further weakening

the effective force-bearing area of the cross-section. 2. Section loss → Decreased bearing capacity: The rate of section loss of reinforcing bars increases, the efficiency of prestress transmission decreases, and the ultimate bearing capacity of the beam body drops. When the area of concrete section spalling exceeds 10%, the height of the compression zone decreases and the flexural bearing capacity declines. The interrelationship chain among the three can be summarized as follows: crack propagation → intensified cross-sectional damage → reduced effective load-bearing section → degradation of bearing capacity. Therefore, crack characteristics and section loss will interact with each other and jointly reduce the bearing capacity of prestressed concrete structures. Therefore, after completing the identification and feature extraction of bridge cracks, the decrease in the compressive capacity of components caused by the section loss in the compression zone and the increased risk of shear failure caused by the shear section loss should also be considered. In order to accurately evaluate the current safety performance of bridge structures, provide the targeted technical basis for maintenance and reinforcement, reveal the evolution law of prestressed concrete structure performance, realize cross-scale mapping from pixel-level image analysis to engineering mechanics response, and solve the core problem of the influence of cracks and section loss on the bearing capacity of concrete; the study further explores the correlation between bridge cracks, section loss and prestressed concrete bearing capacity. The analysis roadmap is shown in Figure 4.

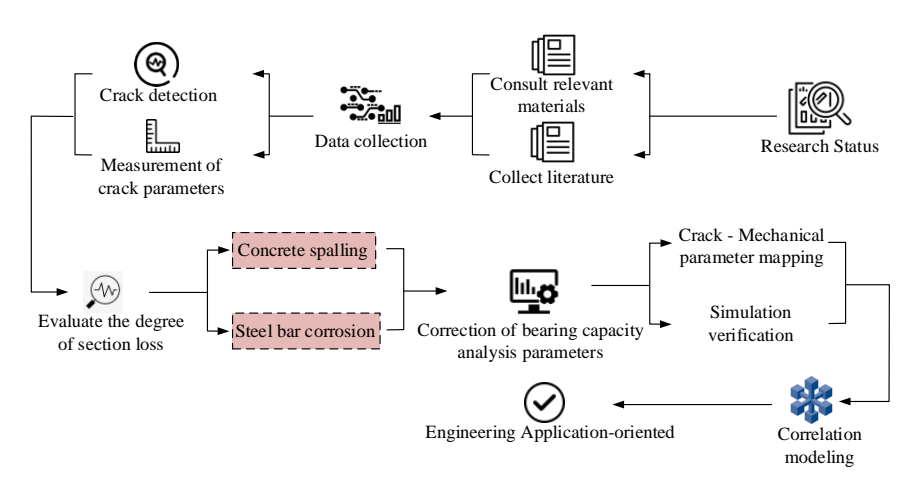


Figure 4. Correlation exploration and analysis roadmap

As illustrated in Figure 4, the approach outlined in the study begins by reviewing relevant materials to establish a theoretical foundation for the research. Then, data collection is carried out, and crack detection and crack parameter measurement are carried out based on the data collected. Then, the degree of section loss is evaluated by detecting concrete spalling and steel bar corrosion rate. After comprehensively considering the synergistic effect of the two, the obtained data is corrected with the bearing capacity analysis parameters, and then, the mechanical parameters of cracks and section loss are mapped and simulated for verification,

and correlation modeling is carried out, and finally, the engineering application is realized, completing the transformation from research to engineering practice. The bearing capacity detection of prestressed concrete is a key technology in the field of bridge engineering, but the traditional method relies on empirical formulae, and there are problems, such as high cost and low efficiency. Therefore, the study introduces LSTM combined with GAN, processes time series data through memory units, captures long-term dependencies, and solves the problem of insufficient detection data, as shown in Figure 5.

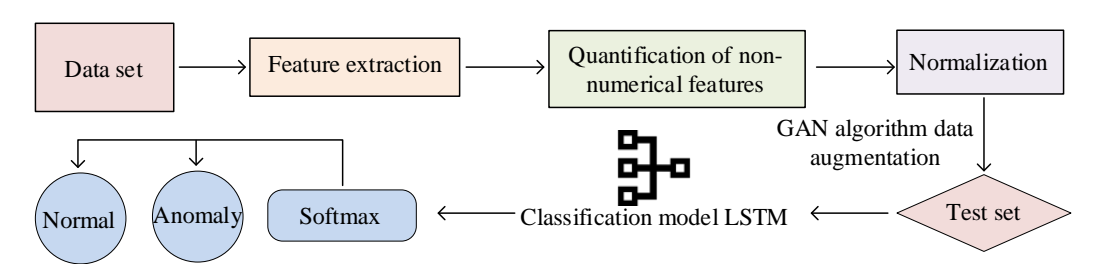


Figure 5. The bearing capacity analysis process combining GAN and LSTM

As shown in Figure 5, the study integrates various discrete monitoring data into a continuous data stream for bridge-related monitoring data, then extracts the key features that affect the bearing capacity of bridge prestressed concrete, and then normalizes the data to eliminate the dimension effect. Subsequently, the GAN algorithm is introduced to enhance the normalized data, generate more diverse samples to expand the dataset, and then form a test set. The processed test set is input into the LSTM model, and the bridge data characteristics are analyzed by using the LSTM's learning ability for time series data. Finally, the Softmax function is used for classification to determine whether the state of the bridge prestressed concrete structure is normal or abnormal, thereby providing a basis for bridge bearing

capacity assessment and maintenance. The normalization operation process is shown in Equation (7).

$$x' = \frac{x - x_{\min}}{x_{\max} - x_{\min}} \tag{7}$$

In Equation (7), x represents the raw data, and x_{max} and x_{min} are the maximum and minimum values of the data, respectively. This step is used for preprocessing the bridge monitoring data to improve the model's training performance. In GAN, the generator G and the discriminator D undergo adversarial training to enhance the objective, as shown in Equation (8).

$$\min_{G} \max_{D} E_{x \square \ pdata(x)} \left\lceil \log D(x) \right\rceil + E_{z \square \ p(z)} \left\lceil \log 1 - D(G(z)) \right\rceil \tag{8}$$

In Equation (8), x represents the raw data, z represents noise, pdata(x) represents the real data distribution, and p(z) represents the noise distribution. Finally, the Softmax converts the raw scores output by the LSTM into probabilities to assess the bearing capacity state of the prestressed concrete bridge. The Softmax operation flow is shown in Equation (9).

$$\sigma(z)_{j} = \frac{e^{zj}}{\sum_{k=1}^{K} e^{z}k}$$

In Equation (9), z represents the input vector, K represents the number of output categories, and z_j represents the j-th input value. Through the operation of the Softmax function, these raw scores are converted into a probability distribution, where the value of each element lies between (0,1), and the sum of all elements' probabilities equals 1, thus representing the probability

that the input sample belongs to each category. Based on the methods for bridge crack recognition, crosssectional loss, and feature parameter extraction, as well as prestressed concrete bearing capacity detection, the study proposes a prestressed concrete bearing capacity analysis model, named OCPGL, which integrates Otsu-Canny, PSO, GAN, and LSTM algorithms. The specific structure of this model is shown in Figure 6.

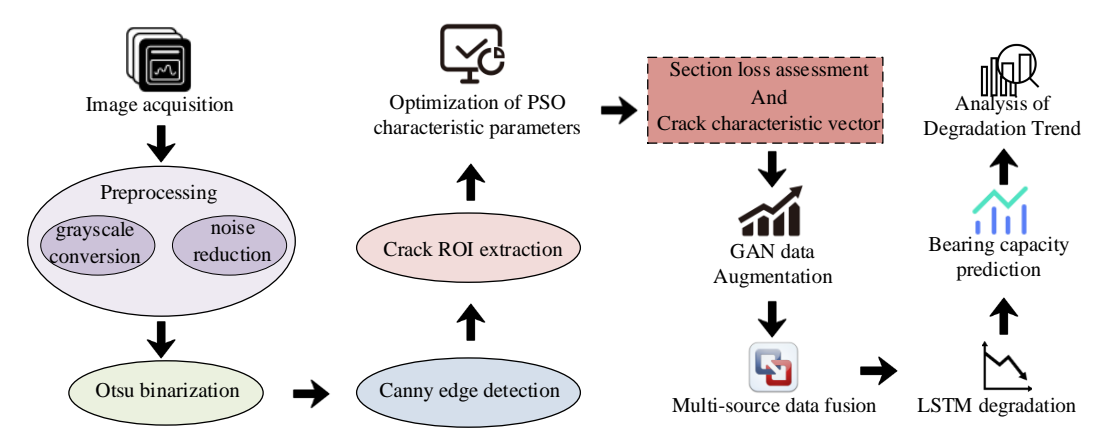


Figure 6. Specific structure diagram of OCPGL analysis model

As shown in Figure 6, OCPGL integrates multiple technologies to achieve full-chain analysis. First, the Otsu-Canny algorithm is used to identify and extract crack feature parameters, and then, the PSO algorithm is used to select core features from redundant features, and the core features of the cracks are fused and evaluated with the cross-sectional loss. Then, the GAN algorithm is used to generate multiple enhanced data to cover extreme working conditions and solve the small sample problem. Finally, the LSTM model is constructed to integrate multi-dimensional data and input it by quarterly sampling, and then, the bearing capacity degradation rate is output to provide a quantitative basis for maintenance and improve the level of intelligent monitoring. When the PSO algorithm performs the feature screening objective function, the goal is to maximize the sum of the correlation coefficients between the feature and the bearing capacity degradation rate. Its calculation process is shown in Equation (10).

$$f(x) = \sum_{i=1}^{n} x_i \square \rho_i$$
 (10)

In Equation (10), x_i represents the feature selection indicator, ρ_i represents the correlation coefficient between the *i*-th crack feature and the degradation rate, and *n* represents the total number of features. The core of LSTM lies in controlling the memory of information through gating mechanisms. The cell state update calculation is shown in Equation (11).

$$C_{t} = f_{t} \square C_{t-1} + i_{t} \square \tilde{C}_{t}$$

(11)

In Equation (11), C_t represents the current cell state, \Box represents element-wise multiplication, C_{t-1} represents discarding old information through the forget gate, and \tilde{C}_t represents adding new candidate information through the input gate, f_t is the output value of the forget gate, i_t is the output value of the input gate. The LSTM prediction result is then corrected based on the "Highway Reinforced Concrete and Prestressed Concrete Bridge and Culvert Design Code," as shown in Equation (12).

$$y_{corr} = y_{pred} \left[1 - \frac{\alpha \Box \omega + \beta \Box d}{f_{ck}} \right]$$
 (12)

In Equation (12), ω represents the crack width, d represents the crack density, α and β represent the empirical coefficients from the code, f_{ck} represents the standard value of the concrete axial compressive strength, and y_{tyred} represents the predicted result.

Prestressed Concrete Bearing Capacity Analysis Based on Bridge Cracks

Feature Analysis and Prediction of Bridge Cracks

In order to verify the superiority of the Otsu-Canny edge detection algorithm, the study compared it with three edge detection algorithms: Robert Cross Gradient Operator (Robert), Sobel operator (Sobel), and Laplace operator (Laplacian). The experimental system version used Windows 11, the operating system was Ubuntu 22.04 OS, the programming language was Python 3.8,

the graphics card was NVIDIA GeForce RTX 4070, and the memory was 64GB. The core software and toolkits used in the experiment include: 1. Image processing tool: OpenCV 4.8.0(for crack image preprocessing, edge detection and contour extraction); 2. Deep learning framework: PyTorch 2.0.1(for implementing Otsu-Canny algorithm optimization, GAN data augmentation, and LSTM model training); 3. Data analysis tools: NumPy 1.24.3 (for numerical computation), Pandas 1.5.3(for dataset management); 4. Visualization tools: Matplotlib 3.7.1(used for drawing algorithm accuracy curves, false detection rate comparison charts,... etc.).

The experimental datasets were the BSD500 dataset and the BSD-Noisy dataset. BSD500 was the gold standard dataset in the field of edge detection and image segmentation, containing 500 natural images. BSD-Noisy was created by artificially adding noise to BSD500. The study conducted accuracy tests on extracting characteristic parameters of concrete cracks (i.e., the number and size of cracks) using four edge detection algorithms; namely, Otsu-Canny, Robert, Sobel, and Laplacian, respectively in the BSD500 and BSD-Noisy datasets. The test results are shown in Figure 7.

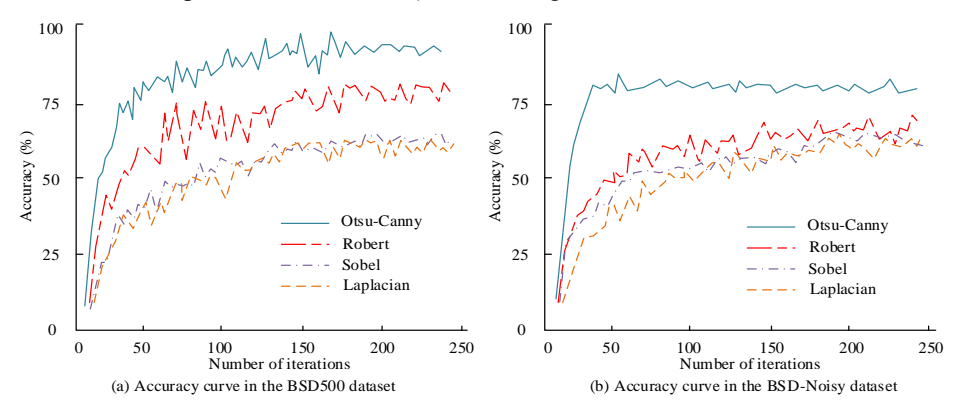


Figure 7. Comparison of the accuracy of extracting characteristic parameters of concrete cracks

As shown in Figure 7(a), when training on the BSD500 dataset, the accuracy of Otsu-Canny reached 76.2% after 50 iterations. The overall accuracy gradually stabilized after 80 iterations, reaching 89.5%. Robert's accuracy fluctuated the most between 50 and 100 iterations, with the highest and lowest values reaching 73.8% and 54.7%, respectively. As shown in Figure 7(b), when training on the BSD-Noisy dataset, the overall accuracy curve of Otsu-Canny converged faster, gradually stabilized after 50

iterations, and the highest accuracy was 78.3%. In conclusion, the Otsu-Canny edge detection algorithm demonstrated superior accuracy, stronger convergence, and minimal fluctuations as the number of iterations increased, outperforming the other algorithms by a significant margin. To further assess the robustness of the Otsu-Canny algorithm, the study performed noise-resistance comparison tests on all four algorithms using noisy images. The results of these tests are presented in Figure 8.

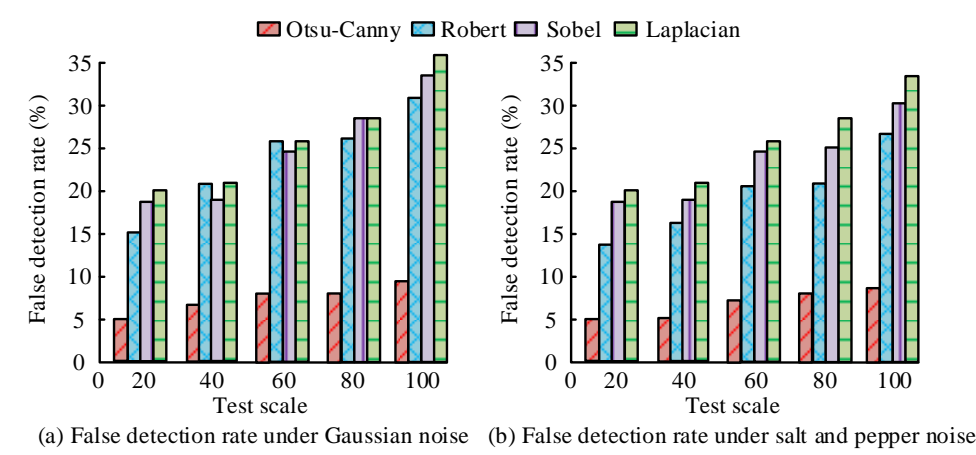


Figure 8. Comparison of noise immunity test results in noisy images

As shown in Figure 8(a), when the test scale was 20, the false detection rate of Otsu-Canny was 5% for images processed with Gaussian noise. As the test scale increased, the false detection rate of the Otsu-Canny algorithm only increased slightly. When the test scale reached 100, its highest false detection rate was 9%. The other three comparison algorithms all showed high false detection rates when processing images with Gaussian noise. The highest false detection rates of Robert, Sobel, and Laplacian were 30%, 33%, and 35%, respectively.

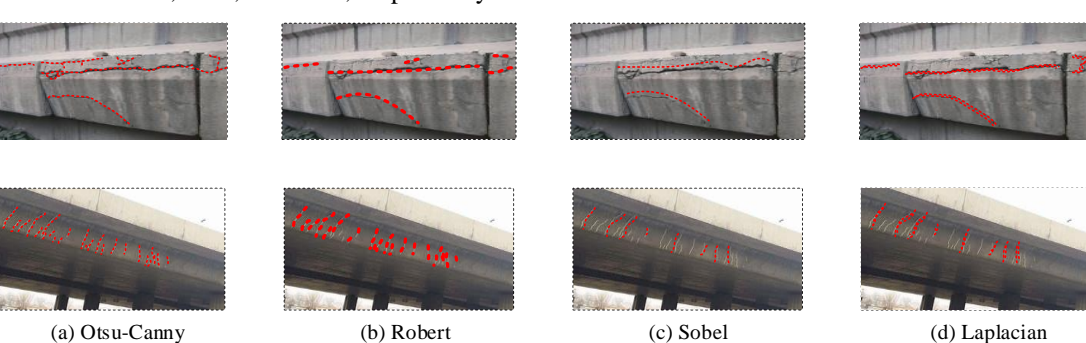


Figure 9. Crack identification visualization display

As shown in Figure 9(a), the Otsu-Canny edge detection algorithm retained real cracks, produced few pseudo-edges, and achieved a detection accuracy of 98.5%. As shown in Figure 9(b), Robert was sensitive to noise, the detected edges appeared coarse, the positioning accuracy was limited, and some edge details were easily lost, resulting in a detection accuracy of 85.2%. As shown in Figure 9(c), the Sobel algorithm missed a large amount of real crack distribution data of bridges. The detected crack positions showed low overlap with the actual cracks, making it less effective in bridge crack monitoring. As shown in Figure 9(d), Laplacian responded strongly to image grayscale mutations and was also highly sensitive to noise, generating a large number of pseudo-edges that interfered with the identification of actual crack distributions, and caused significant edge offset. In summary, the Otsu-Canny edge detection algorithm accurately detected the distribution of transverse and longitudinal cracks in bridges and performed better than the other algorithms.

Quantification of Section Loss in Bridge Deck Cracks and Experimental Validation

After verifying the performance of the Otsu-Canny

edge detection algorithm, the study further evaluated the performance of the prestressed concrete bearing capacity analysis model OCPGL by comparing it with three analysis models: Convolutional Neural Network-Long Short-Term Memory Network (CNN-LSTM), Gated Recurrent Unit-Dense Layer (GRU-Dense), and Radial Basis Function-Support Vector Machine (RBF-SVM). The experiment used a Donghua static test strain gauge for signal acquisition. A 40 kN through-hole jack served as the hydraulic pump, and a rubber-based foil resistance strain gauge was employed for strain measurement. The collected strain signals and bearing capacity data were preprocessed (filtered and denozed) by DHDAS 6.0, the supporting software of Donghua test. The subsequent data analysis (such as the calculation of mean square error and the solution of the coefficient of determination R2) was accomplished through the Statistics and Machine Learning Toolbox of MATLAB 2023a, and the visualization of the deflection curve simulation results was implemented using OriginPro 2023b. The raw-material parameters of the prestressed concrete design experiment are listed in Table 1.

As shown in Figure 8(b), the Otsu-Canny edge detection algorithm still demonstrated excellent robustness when

processing images with salt and pepper noise, with a

maximum false detection rate of 7%. In summary, Otsu-

Canny exhibited strong robustness when facing different

types of noise and showed significant advantages in

noise resistance under complex noise environments. In

order to further verify the recognition performance of

the Otsu-Canny algorithm on actual bridge cracks, the

study conducted a visualization test of crack

recognition, and the results are shown in Figure 9.

Classification Project		Symbol	Unit	Data
Prestressed concrete	Length	L	cm	600
	Height	Н	cm	40
	Axial compressive design strength	f_{cd}	MPa	18.5
	Axial tensile design strength	f_{td}	MPa	1.68
	Diameter	d	mm	6
Ordinary reinforcing bars	Elastic modulus	Es	MPa	2.2*105
	Standard value of tensile strength	f_{sk}	MPa	245

Table 1. Prestressed concrete experimental raw-material parameters

As shown in Table 1, the selected prestressed claymixed concrete beam had a length of 600 cm and a height of 40 cm. Its compressive strength was 18.5 MPa, and its tensile strength was 1.68 MPa. The inner diameter of the steel bar was 6 mm, with a tensile strength of 2.1×10^5 MPa and an abrasion resistance of

245 MPa. The accuracy of OCPGL's prediction performance was verified under identical factory conditions. Four types of model were studied. As the existing structural condition deteriorated, the crack width increased to 0.5 mm. The results produced ten sets of comparative outcomes.

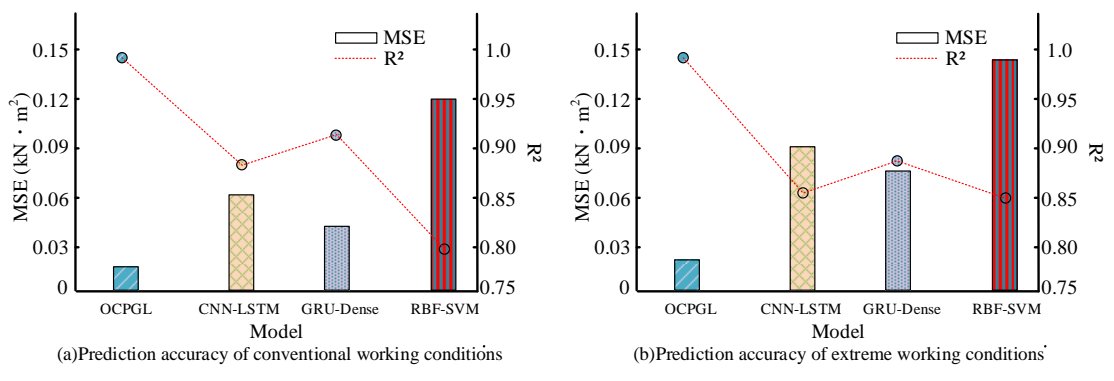


Figure 10. Prediction accuracy test results under extreme conditions

As shown in Figure 10(a), under normal working conditions, the Mean Square Error (MSE) of the bearing capacity predicted by OCPGL was only 0.015 kN·m², and its Coefficient of Determination (R²) was 0.98. The MSE of the GRU-Dense model was slightly higher than that of OCPGL, reaching 0.045 kN·m², with an R² of 0.88. The bearing capacity MSE of CNN-LSTM and RBF-SVM was much higher than that of the previous two models, reaching 0.068 kN·m² and 0.12 kN·m², respectively. As shown in Figure 10(b), under extreme working conditions, the MSE and R² of OCPGL did not change significantly, remaining at 0.018 kN·m² and 0.97, respectively. When subjected to extreme working conditions, the MSE of the other three models increased by about 40%, and their R² values dropped below 0.9. In summary, the proposed model demonstrated better bearing capacity prediction accuracy under both normal and extreme conditions. To further verify the effect of OCPGL on the bearing capacity analysis of prestressed

concrete in actual bridges, the deflection curve simulation values of the four models were experimentally compared, and the results are shown in Figure 11.

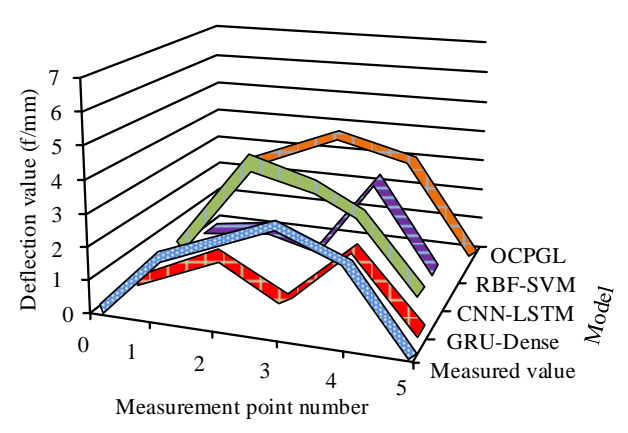


Figure 11. Deflection curve simulation results

As shown in Figure 11, the measured deflection value at point 1 was 2f/mm, the deflection value at point 2 was 2.5f/mm, and the deflection value at point 3 reached 3.1f/mm. Among the four comparison models, only the predicted values of OCPGL were consistent with the actual values. The deflection value at point 1 was 2f/mm, the deflection value at point 2 was 2.4f/mm, and the deflection value at point 3 was 3f/mm, with a prediction accuracy of up to 96.5%. The prediction values of the other three models deviated significantly. The experimental results demonstrated that OCPGL provided a more reliable basis for bearing capacity assessment and deformation control of prestressed concrete structures in actual engineering by accurately predicting the key characteristic points and overall trends of the deflection curve. Its stability and accuracy in complex engineering scenarios were far superior to

those of the comparison models.

Verification of the Correlation between Cracks, Section Loss and Bearing Capacity

The above experimental results have confirmed the high accuracy of the OCPGL model in bearing capacity prediction, and the core advantage of this model lies in the deep integration of the correlation between cracks, section loss and bearing capacity. To further verify that this correlation is not an accidental result of model fitting, but an inherent law of prestressed concrete structures, the study conducted loading experiments on 120 groups of prestressed concrete beam specimens, measuring the corresponding values of different crack widths, steel bar corrosion rates and ultimate bearing capacity. The results are shown in Table 2.

1	Table 2. Measured cor	correlation data of cracks, section loss and bearing capacity on Proportion of concrete Ultimate bearing Decline rate			
dth	Steel bar corrosion	Proportion of concrete	Ultimate bearing	Decline rate	

Crack width (mm)	Steel bar corrosion rate (%)	Proportion of concrete spalling area (%)	Ultimate bearing capacity (kN)	Decline rate of bearing capacity (%)
0.1	1.2	2.1	485	1.0
0.3	4.5	5.3	462	5.6
0.5	8.9	8.7	431	12.1
0.8	15 3	12.5	398	19.6

The data in Table 2 is derived from the loading experiments of 120 sets of full-scale prestressed concrete beam specimens. The parameters of the specimens are referred to in Table 1 (the axial compressive design strength of the concrete is 18.5MPa, and the diameter of the reinforcing bars is 6mm). Among them, the crack width is the maximum crack width on the surface of the specimen (accuracy ± 0.01 mm); The corrosion rate of reinforcing bars is the cross-sectional loss rate (corrosion area/original cross-sectional area, measured by electrochemical impedance spectroscopy, with an error of $\pm 0.2\%$). The proportion of concrete spalling area is the ratio of the spalling area to the total cross-sectional area of the specimen (calculated by image segmentation method). The ultimate bearing capacity is the maximum load at which the specimen fails (measured by a 40kN through-hole jack). The rate of decline in bearing capacity is calculated with reference to the benchmark specimen without cracks and no cross-sectional loss (ultimate bearing capacity 490kN). The data in the table directly reflects the

synchronous variation law of crack propagation, intensified section loss and degradation of bearing capacity.

DISCUSSION

In recent years, the latest research in the field of crack detection and feature extraction has further promoted the development of crack detection technology. For instance, scholars, such as Nguyen, S.D. et al., systematically compared deep learning algorithms and found that ResNet/DenseNet performed best in crack classification, FasterR-CNN in object detection, and pix2pix in segmentation tasks. However, their research focused on asphalt pavement and remained at the level of "crack recognition accuracy". The association between crack characteristics and internal damage of pavement structures was not established, let alone extended to bearing capacity assessment (Nguyen et al., 2023). Although the research of Umar et al. demonstrated the application of CNNs and RNNs in the

crack detection of photovoltaic panels, pointing out the limitations of traditional methods, such as low efficiency and high error rate, the research object was homogeneous materials, like photovoltaic panels, and it did not involve the mapping of characteristic parameters and structural performance (Umar et al., 2024).

However, the current research on the bearing capacity of prestressed concrete also faces bottlenecks, such as "mechanism simplification" and "data limitations". Although Mari et al. established a nonlinear time-correlation model considering the influence of corrosion and analyzed the weakening of bearing capacity and stiffness caused by corrosion, their model was only for frame structures and did not quantify the dynamic correlation between crack propagation and steel bar corrosion. It only regarded corrosion as an independent variable and ignored the key coupling effect that "cracks provide channels for corrosive media" (Mari et al., 2022). Yang et al. generated 4165 sets of virtual data through finite element simulation and constructed a prediction model for the bearing capacity of rusted prestressed concrete beams. However, relying on a virtual database, their study lacks the coupling analysis of actual crack characteristics and the degree of rusting, and their model does not incorporate the bearing capacity degradation law under sequential loads, making it difficult to reflect the performance of the structure throughout its life cycle (Yang et al., 2023; Adam et al.,

Overall, existing studies either focus on crack detection in a single scenario or emphasize the independent impact of corrosion on bearing capacity, but none of them have formed a complete chain of "crack feature extraction → quantification of section loss → dynamic prediction of bearing capacity". The innovation of the research is reflected in the following aspects: 1. For the first time, the quantitative relationship between crack width and steel bar corrosion rate, section loss and bearing capacity decrease was quantified, filling the theoretical gap of "crack morphology - structural damage - mechanical properties", and it has more engineering guidance value than the qualitative analysis of Mari et al. 2. By organically integrating the precise detection of Otsu-Canny, the feature screening of PSO, the data augmentation of GAN and the time-series modeling of LSTM, it not only solves the problem of "insufficient data in semi-supervised learning" pointed out by Nguyen et al., but also overcomes the limitations of Yang et al.'s virtual data, achieving a deep coupling of algorithm advantages and physical mechanisms.

CONCLUSION

In view of that traditional prestressed concrete bearing capacity analysis methods ignore the intrinsic correlation between cracks, section loss and bearing capacity, and have incomplete crack feature extraction, low efficiency of multi-source data fusion and insufficient long-term prediction accuracy, this study not only designed the OCPGL prestressed concrete bearing capacity analysis model, but also revealed the cascading influence mechanism of the three through experiments. It provides a complete basis from observation" "phenomenon "mechanism quantification" for the assessment of carrying capacity. This model automatically completes crack edge detection and double-threshold optimization through the Otsu-Canny algorithm, uses the PSO algorithm to screen the core correlation features of crack-section loss to reduce data redundancy, generates enhanced data under extreme working conditions with the help of GAN to improve the generalization ability of the model, and captures the bearing capacity degradation time-series law based on the correlation mechanism through the LSTM network, thus effectively solving the problem of nonlinear prediction in complex stress environments. The experimental results demonstrated that the accuracy of the Otsu-Canny algorithm reached 89.5% after several iterations, with the highest false detection rate of bridge cracks under different noise impacts reaching 9%. The detection accuracy for different types of crack was as high as 98.5%. Regarding the OCPGL evaluation, the model's bearing capacity MSE was only 0.015 kN·m², with an R² of 0.98. The prediction accuracy for the deflection curves at various bridge measurement points was up to 96.5%. In terms of the correlation mechanism, the crack width is significantly positively correlated with the corrosion rate of reinforcing bars. When the crack width exceeds 0.2mm, the corrosion rate significantly accelerates. The increase in the corrosion rate of steel bars, the decrease in bearing capacity, the increase in the proportion of concrete spalling area, and the decrease in bearing capacity confirm that cracks significantly reduce bearing capacity by intensifying cross-sectional loss. Overall,

the core value of OCPGL lies in transforming the quantitative correlation among cracks, section loss, and bearing capacity into a computable predictive model. It demonstrates an accurate ability to depict the correlation rules under various load conditions, noise environments, and data-scarce scenarios. However, limited by current experimental conditions, the model's ability to

REFERENCES

- Alam, M.A., Rahman, M.M., & Islam, J. (2023). Optimal shear strengthening of severely deficient RC beam using JFRP laminate with anchor. *Jordan Journal of Civil Engineering*, 17(4), 723-738.
- Alhebrawi, M.N., Huang, H., & Wu, Z. (2023). Artificial intelligence enhanced automatic identification for concrete cracks using acoustic impact hammer testing. *Journal of Civil Structural Health Monitoring*, 13(2), 469-484.
- Choi, K.H., & Ha, J.E. (2023). An adaptive threshold for the Canny edge with actor-critic algorithm. *IEEE Access*, 11, 67058-67069.
- Demir, S., & Sahin, E.K. (2023). Predicting occurrence of liquefaction-induced lateral spreading using gradient boosting algorithms integrated with particle swarm optimization: PSO-XGBoost, PSO-LightGBM, and PSO-CatBoost. *Acta Geotechnica*, 18(6), 3403-3419.
- Fan, Z., Bai, K., & Chen, C. (2024). Ultrasonic testing in the field of engineering joining. *The International Journal of Advanced Manufacturing Technology*, 132(9), 4135-4160.
- Farneti, E., Cavalagli, N., Costantini, M., Trillo, F., Minati, F., Venanzi, I., & Ubertini, F. (2023). A method for structural monitoring of multispan bridges using satellite InSAR data with uncertainty quantification and its pre-collapse application to the Albiano-Magra Bridge in Italy. Structural Health Monitoring, 22(1), 353-371.
- Farzana, K.A., Ahmed, K.S., Ahmed, M., Ansary, M.A., & Abedin, M.Z. (2024). Vertical bearing capacity of spun precast concrete piles in liquefiable soil: A case study. *Geotechnical Research*, 11(2), 66-80.
- Gleich, P., & Maurer, R. (2023). Arch action model for the structural assessment of existing prestressed concrete bridges. *Structural Concrete*, 24(5), 5827-5838.
- Hu, X., Xue, W., & Zheng, R. (2024). Hysteretic performance of prestressed concrete beams with AFRP tendons under cyclic loading. *Structural Concrete*,

generalize to rare working conditions, such as extreme corrosion or sudden overloads, still requires more engineering data. Future work will focus on model lightweight optimization and hardware adaptation, promoting its practical application in bridge health monitoring systems.

- 25(1), 620-636.
- Li, Y., Sun, K., Si, Z., Chen, F., Tao, L., Li, K., & Zhou, H. (2024). Monitoring and identification of wire breaks in prestressed concrete cylinder pipe based on distributed fiber optic acoustic sensing. *Journal of Civil Structural Health Monitoring*, *14*(1), 3-14.
- Liu, L., Liu, Z., Hou, A., Qian, X., & Wang, H. (2024).
 Adaptive edge detection of rebar thread head image based on improved Canny operator. *IET Image Processing*, 18(5), 1145-1160.
- Marí, A., Bairán, J.M., Oller, E., & Duarte, N. (2022). Modeling serviceability performance and ultimate capacity of corroded reinforced and prestressed concrete structures. *Structural Concrete*, 23(1), 6-15.
- Nguyen, S.D., Tran, T.S., Tran, V.P., Lee, H.J., Piran, M.J., & Le, V.P. (2023). Deep learning-based crack detection: A survey. *International Journal of Pavement Research and Technology*, 16(4), 943-967.
- Ni, Y.H., Wang, H., Mao, J.X., Xi, Z., & Chen, Z.Y. (2025). Quantitative detection of typical bridge surface damages based on global attention mechanism and YOLOv7 network. *Structural Health Monitoring*, 24(2), 941-962.
- Ramadhan, R.P., Pahrizal, P., & Apridiansyah, Y. (2025). Eksperimen perbandingan Otsu thresholding dan Canny edge detection terhadap peningkatan kualitas citra beresolusi rendah. *Ranah Research: Journal of Multidisciplinary Research and Development*, 7(3), 2210-2216.
- Salunke, D., Tekade, P., Ranjan, N., Ujalambkar, D., Sangve, S., & Mane, D. (2023). Real-time dimension detection using customized Canny edge detection algorithm. *International Journal of Engineering Trends* and Technology, 71(9), 375-384.
- Syahfitri, N.N.A. (2023). Digital image processing on kaffir orange peel with Canny edge detection algorithm. Journal of Artificial Intelligence and Engineering Applications, 3(1), 315-322.
- Tonelli, D., Rossi, F., Brighenti, F., Verzobio, A., Bonelli, A., & Zonta, D. (2023). Prestressed concrete bridge

- tested to failure: The Alveo Vecchio viaduct case study. *Journal of Civil Structural Health Monitoring*, 13(4), 873-899.
- Triwibowo, D.N., Dewa, B.P., Sumantri, R.B.B., & Suryani, R. (2023). Identification of breast tumors with image processing using Canny edge detection. *Journal of Advanced Health Informatics Research*, 1(1), 28-34.
- Umar, S., Nawaz, M.U., & Qureshi, M.S. (2024). Deep learning approaches for crack detection in solar PV panels. *International Journal of Advanced Engineering Technologies and Innovations*, 1(3), 50-72.
- Usman, A.M., & Abdullah, M.K. (2023). An assessment of building energy consumption characteristics using analytical energy and carbon footprint assessment model. *Green and Low-Carbon Economy*, 1(1), 28-40.
- Xiong, J., Wang, D., Yin, J., & Wu, R. (2025). Precise Z-

- Block positioning and dimension measurement using improved Canny edge detection and sub-pixel contour fitting. *The Journal of Supercomputing*, 81(1), 26-31.
- Yang, Z., Lei, Y., & Li, G. (2023). Experimental and finite element analysis of shear behavior of prestressed high-strength concrete piles. *International Journal of Civil Engineering*, 21(2), 219-233.
- Zhang, Y., Hu, Q., Li, D., Luo, H., & Li, W. (2024). Texture feature-based local adaptive Otsu segmentation and Hough transform for sea-sky line detection. *Multimedia Tools and Applications*, 83(12), 34477-34498.
- Zhou, H., Han, S., Liu, Y., & Wang, H. (2025). Research on fatigue residual bearing capacity of prestressed concrete beams considering size effect. *Ce/Papers*, 8(2), 262-268.